Rapid Communications

Ab initio current-induced molecular dynamics

Jing-Tao Lü,[1] Susanne Leitherer,[2] Nick R. Papior,[3] and Mads Brandbyge[2]

[1]*School of Physics and Wuhan National High Magnetic Field Center, Huazhong University of Science and Technology, 430074 Wuhan, China*

[2]*Department of Physics, Technical University of Denmark, DK-2800 Kongens Lyngby, Denmark*

[3]*DTU Computing Center, Department of Applied Mathematics and Computer Science, Technical University of Denmark, DK-2800 Kongens Lyngby, Denmark*

(Received 18 January 2020; accepted 30 April 2020; published 18 May 2020)

We extend the *ab initio* molecular dynamics (AIMD) method based on density functional theory to the nonequilibrium situation where an electronic current is present in the electronic system. The dynamics is treated using the semiclassical generalized Langevin equation. We demonstrate how the full anharmonic description of the interatomic forces is important in order to understand the current-induced heating and the energy distribution both in frequency and in real space.

DOI: 10.1103/PhysRevB.101.201406

Introduction. Energy dissipation from an electronic current into the motion of atoms is an important and challenging scientific and technological problem [1,2]. Especially, conductors consisting of a few atoms can be driven into a highly nonequilibrium vibrational state by a current [3,4]. The local excitation of the atomic vibrations is hard to address in experiments [5–10] and theoretically [11–14]. So far, the formation of atomic "hot spots" has been demonstrated using first-principles calculations at the level of density functional theory (DFT) using the harmonic approximation thus neglecting intermode coupling [15]. It was also shown how current-induced momentum transfer ("electron wind" forces) may displace the hot spots up- or downstream with respect to the current. This behavior has been observed in recent experiments [16,17]. In a simplified picture one may consider the atomic motion in the conductor to have a higher effective temperature compared to the surrounding electrodes [4,18]. However, the fact that individual vibrational modes couple differently to the electronic current and phonon reservoirs makes this picture invalid in general. Moreover, the anharmonic intermode coupling distributes the energy among these and makes the problem challenging to treat beyond model calculations.

Here, we present a computational method which allows for *ab initio* molecular dynamics (AIMD) simulation of atomic scale conductors in the presence of electronic current at low temperature where the quantum effect is important. It can address the effects of the current on the vibrational excitation (Joule heating), the current-induced "wind" forces, the coupling to electrode phonon reservoirs [19], and the anharmonic couplings between the modes of the conductor [20]. We demonstrate the method on two "benchmark" atomic scale conductors, an atomic gold chain and a benzene molecule, and analyze the role of the individual effects for the dissipation.

Langevin equation. We consider an atomic scale conductor consisting of a central bottleneck junction and two electrodes, "left" and "right," respectively. In the presence of an electrical current, electrons are scattered near the junction and deposit energy to the surrounding atoms. We are interested in the atomic dynamics driven by the electrical current across the junction. To this end, we define the "system" as the coordinates of the nuclei in the junction. All remaining degrees of freedom (DOF) are treated as reservoirs/baths. We consider two kinds of reservoirs. The first is the electronic one, including all the electron DOF in the conductor and electrodes. Importantly, in the presence of electrical current, the electron reservoir is in a nonequilibrium state. This nonthermal reservoir serves as the energy source, depositing energy to the atoms. The second kind is the phonon reservoirs of the left and right electrode parts.

Employing the Feynman-Vernon influence functional approach, a semiclassical generalized Langevin equation (SCGLE) can be derived to describe the dynamics of the nonequilibrium system [14,21–25],

$$\ddot{\boldsymbol{Q}}(t) = \boldsymbol{F}[\boldsymbol{Q}(t)] + \int_{-\infty}^{t} \boldsymbol{\Pi}^{r}(t-t')\boldsymbol{Q}(t')dt' + \boldsymbol{f}(t). \quad (1)$$

Here, $\boldsymbol{Q}(t)$ is the mass-normalized displacement of system nuclei away from their equilibrium positions, i.e., $Q_i(t) = \sqrt{m_i}[R_i(t) - R_i^0]$, with i representing the nuclear and its Cartesian index, m_i the nuclear mass, and $R_i(t)$ and R_i^0 the nuclear positions at time t and at equilibrium, respectively. We split the forces acting on the system into different terms. The force $\boldsymbol{F}[\boldsymbol{Q}(t)]$ is obtained from equilibrium DFT, while the corrections due to coupling to reservoirs and the effects of nonequilibrium are reflected in the last two terms on the right-hand side of Eq. (1). We treat this latter coupling perturbatively to linear order in Q [15,26]. Thus we limit ourselves to quasistationary situations where the system is stable on the timescale much longer than the vibrations and the excursions from equilibrium are still small. We neglect here the constant (zero order in Q) current-induced force which can be trivially included and focus on the excitation effects due to the other terms.

In contrast to the classical Langevin approach, the reservoirs are treated fully quantum mechanically in SCGLE. The time nonlocal term describes the backaction of reservoirs on

the system due to finite system displacement $\boldsymbol{Q}$, while $\boldsymbol{f}$ is the fluctuating/stochastic force with zero mean. It can be characterized by the correlation function,

$$\langle \boldsymbol{f}(t)\boldsymbol{f}^T(t')\rangle = \hbar\hat{\boldsymbol{\Pi}}(t-t'), \tag{2}$$

which includes thermal and quantum fluctuations. Both $\hat{\boldsymbol{\Pi}}$ and $\boldsymbol{\Pi}^r$ are given by a sum of contributions, i.e., $\boldsymbol{\Pi}^r = \boldsymbol{\Pi}^r_e + \boldsymbol{\Pi}^r_L + \boldsymbol{\Pi}^r_R$, with e, L, and R representing the electron, the left, and the right phonon reservoirs, respectively.

In nonequilibrium Π^r and $\hat{\Pi}$ can be obtained using nonequilibrium Green's functions [22]. Importantly, they depend on the presence of current: The bias-dependent part of $\hat{\Pi}_e$ generates Joule heating, while Π^r_e contains current-induced forces. In nonequilibrium the fluctuation-dissipation relation linking Π^r and $\hat{\Pi}$ becomes invalid, and the individual magnitudes of Π^r and $\hat{\Pi}$ matter. This is opposed to equilibrium AIMD where one may more freely choose how to describe the coupling to reservoirs which in the end thermalize the system.

Previously, Eq. (1) has been used for *ab initio* calculations in the harmonic approximation [14,15,22]. Here, we go beyond this limitation and perform AIMD simulations by numerically solving Eq. (1), with all parameters obtained from the same DFT setup [27]. Validation of the method and details of the numerical calculation can be found in Ref. [28]. In the following, we consider two prototype atomic conductors and illustrate the importance of anharmonic vibrational coupling on the energy redistribution both in frequency and in real space.

Au chain. The first example is a 5-atom gold chain between two Au(100) electrodes [inset of Fig. 1(a)]. The temperature of the electrodes is 4 K. In the harmonic approximation, Eq. (1) is linear and can be solved directly. We first check that the MD result in the harmonic approximation reproduces that from the direct solution of Eq. (1) (Fig. S1 in Ref. [28]). After validating the method, we proceed to study the energy transfer from the nonequilibrium electronic bath to the system when the applied voltage bias is finite, $V \neq 0$. There are two energy transfer channels: The first is the stochastic Joule heating from the bias-dependent fluctuating force correlation function $\hat{\Pi}_e$. The second is the work done to the system through the energy nonconserving [12] (NC) current-induced forces in Π^r_e. The energy deposited in the system can be further transferred into the left/right equilibrium phonon reservoirs. If the system remains stable it reaches a steady state when the energy into the system is balanced by the energy into the phonon reservoirs.

After reaching a steady state, we use the power spectrum of the velocity-velocity correlation function C_{vv} [Eq. (S1) of Ref. [28]] to characterize the frequency/energy-resolved contribution to the system kinetic energy. Integrating C_{vv} yields the kinetic energy stored in the system for frequencies below ω,

$$E_K(\omega) = \int_0^\omega \frac{d\omega'}{2\pi} C_{vv}(\omega'). \tag{3}$$

The calculated results for C_{vv} along with E_K are shown in Fig. 1(a) for the harmonic calculation using the dynamical matrix from DFT, and in Fig. 1(b) for the full AIMD calculation. Applying a bias voltage results in an increase in

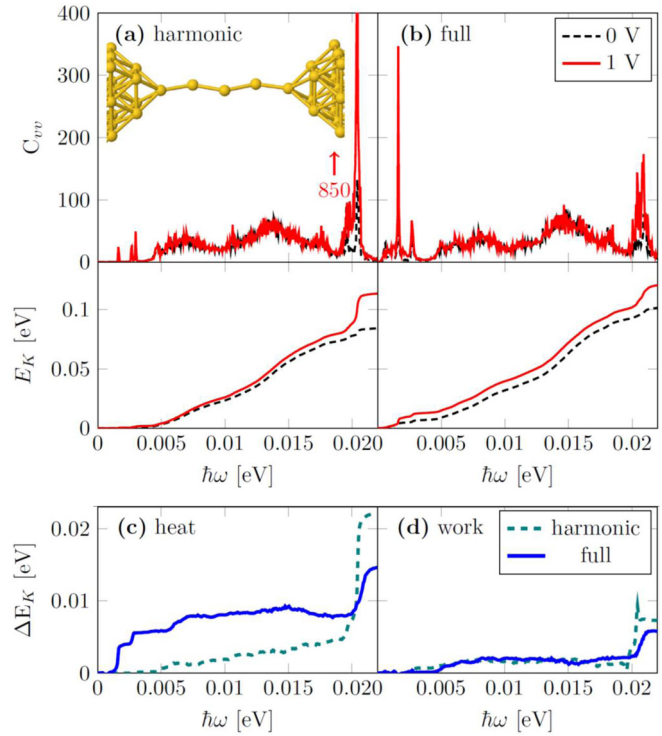

FIG. 1. (a), (b) Power spectra (C_{vv}) and its cumulative integral (E_K) of the 5-atom Au chain connecting to Au(100) electrodes (inset) from MD calculations at a voltage bias of 0 and 1 V. (a) Harmonic calculation using the dynamical matrix. The inset shows the structure of the chain. One layer of the semi-infinite Au(100) electrodes with a cross section of 3×3 atoms is shown on both sides, to which the chain connects via the pyramids. The periodic boundary condition is used in the transverse direction. (b) Full AIMD calculation. (c), (d) The excess kinetic energy ΔE_K (the kinetic energy at nonzero bias subtracted by the zero-bias value) separated into contributions of heat and work. The work is contributed by the current-induced NC force, while the heat is from Joule heating. The coupling of low-frequency modes <4 meV to the electrons was excluded in the calculation. We use a time step of 10 fs in the MD simulation.

vibrational kinetic energy, which can be divided into separate heat and work contributions, shown in Figs. 1(c) and 1(d), respectively. The work part comes from the contribution of NC current-induced forces, while the heat part is from Joule heating.

Comparing results at $V = 0$V (equilibrium) and $V = 1$V (nonequilibrium) from the harmonic approximation, we find that electrons transfer energy mainly to the high-frequency modes at ∼0.02 eV. This is indicated by a big step at ∼0.02 eV at 1 V [red line in the lower panel of Fig. 1(a)]. These modes are the alternating-bond-length (ABL) modes consistent with previous experimental and theoretical studies [10,13,15,26]. In addition to stronger coupling to electrons, the ABL frequencies are located above the bulk phonon band of Au. This hinders a direct harmonic energy transfer to the phonon reservoirs. Inclusion of the anharmonic coupling leads to an energy redistribution from the high- to the low-frequency modes. This is seen from the strongly enhanced heating of the low-frequency modes (<5 meV) in the anharmonic result, which is absent in the harmonic case. The anharmonic

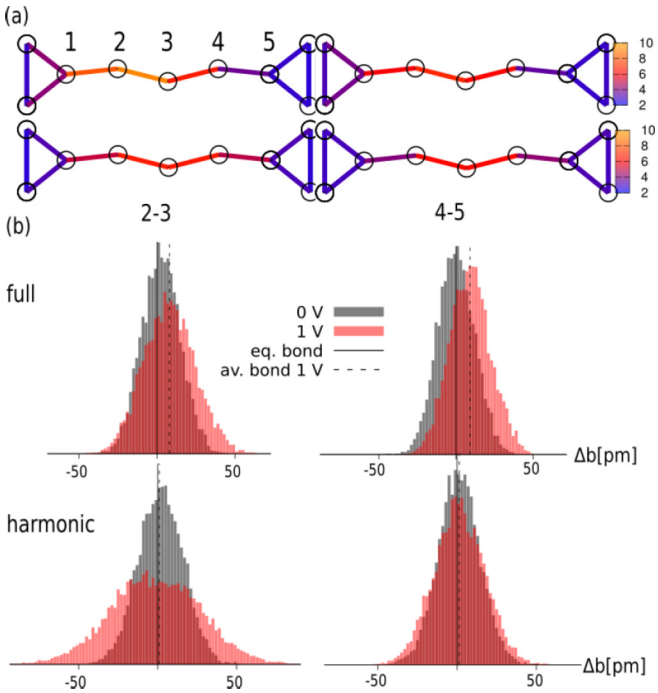

FIG. 2. (a) Comparison of bond kinetic energy in meV from harmonic (left) and full AIMD (right) calculations. Shown is the bond energy at 1 V with (top, asymmetric) and without (bottom, symmetric) NC force. (b) Bond-length distribution between atoms 2-3 and 4-5 calculated from the full AIMD and the harmonic approximation at 0 and 1 V. In the harmonic case, bond 2-3 is strongly broadened at 1 V but the average bond length stays the same. In the full AIMD results, the average bond length increases for both bonds. The broadening of bond distribution is reduced compared to the harmonic case, indicating reduced heating of bonds due to anharmonic intermode coupling. The details of bond changes are summarized in Table I.

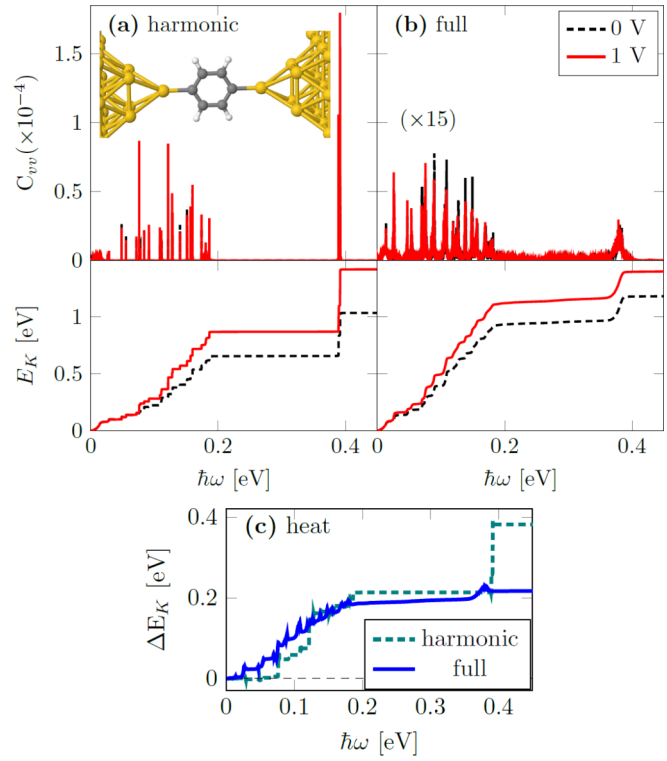

FIG. 3. Power spectra (C_{vv}) and its cumulative integral (E_K) of the benzene molecule connecting to Au electrodes through Au-C bonds. (a) Harmonic calculation using the dynamical matrix. The inset shows the junction geometry. The 5-atom pyramids at both sides connect to the semi-infinite Au(100) electrodes with a 4 × 4 cross section (not shown). The periodic boundary condition is used for the transverse direction. (b) Anharmonic calculation. (c) Comparison of excess kinetic energy from harmonic and anharmonic calculations. The contribution of work from the NC force is negligible in this case.

coupling also reduces the excess kinetic energy in the system by opening an indirect channel of energy transfer from the ABL modes to the bulk electrode phonon reservoirs [Figs. 1(c) and 1(d)].

We now analyze the MD results in real space to gain further understanding of the bond properties. In Fig. 2(a) the kinetic energy per bond [Eq. (S6) of Ref. [28]] is shown for the harmonic and anharmonic cases. In each case, we compare the situations with and without a work contribution from nonconservative current-induced forces. The inclusion of NC current-induced forces leads to a left-right symmetry breaking in the real space energy distribution. Specifically, more energy is accumulated in bonds near the left electrode from where the electrons enter the junction. This asymmetric concentration of energy ("hot spot") was explained by the asymmetric excitation of left- and right-traveling phonon waves by NC current-induced forces [15].

Due to this effect, some bonds in the chain heat up strongly. We have compared the statistics of bond-length fluctuations between atoms 2-3 and 4-5 in both the harmonic and full AIMD calculations [Fig. 2(b) and Table I]. The 2-3 bond shows larger broadening compared to the 4-5 bond in both cases. This is a direct result of asymmetric heating. In the AIMD calculation, the broadening is reduced compared to the harmonic result. This is due to the anharmonic energy transport channel to the phonon reservoirs, consistent with the analysis in Fig. 1. Moreover, we observe elongation of both bonds in the AIMD result. This is another manifestation of anharmonicity [29].

Benzene molecular junction. The second example we consider is a benzene molecular junction connecting to Au(100) electrodes at 4 K through direct Au-C bonds [30] [inset of Fig. 3(a)]. Due to different atomic mass and bonding types, there is a large frequency mismatch between

TABLE I. Current-induced change of average bond length $\Delta l = l(1\text{ V}) - l(0\text{ V})$ and its standard deviation $\Delta\sigma = \sigma(1\text{ V}) - \sigma(0\text{ V})$. Au(2-3) and Au(4-5) are bonds between atoms 2, 3 and 4, 5 in the Au chain, and Au-C, C-C, and C-H are the average of the three kinds of bonds in the benzene junction.

		Au(2-3)	Au(4-5)	Au-C	C-C	C-H
Harmonic	$\Delta\sigma$ (Å)	0.014	0.003	0.009	0.007	0.01
	Δl (Å)	0.0	0.0	0.0	0.0	0.0
Full	$\Delta\sigma$ (Å)	0.004	0.001	0.014	0.003	0.0
	Δl (Å)	0.008	0.009	0.024	0.0	0.0

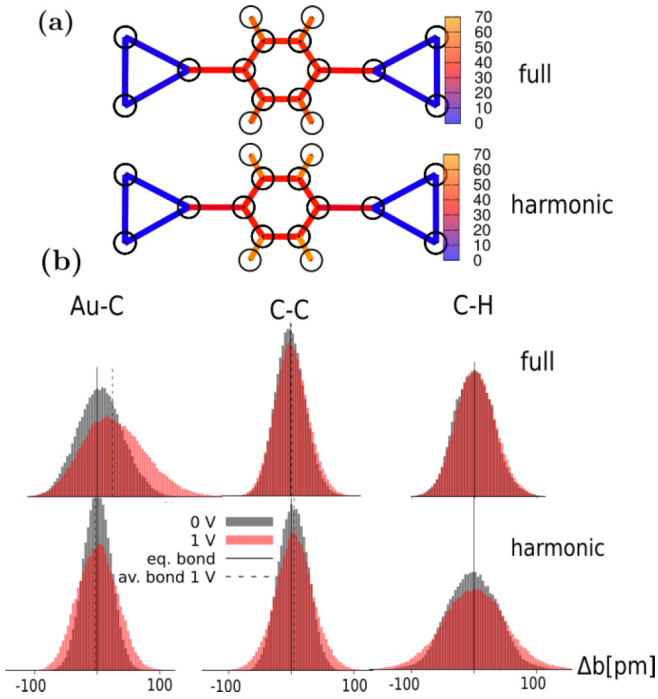

FIG. 4. (a) Comparison of kinetic energy per bond in meV from the full AIMD and the harmonic calculation. (b) Length distribution of different bonds calculated from the two methods. In the harmonic results, all the bonds show a broader distribution at 1 V compared to 0 V. In the full AIMD results, C-C and C-H bonds show little broadening, while the Au-C bond exhibits the widest distribution and an increase of average bond length. The details of the bond changes are summarized in Table I. Interestingly, it also shows a certain skewness with a larger probability to the longer length side.

benzene vibrational modes (0–380 meV) and the gold electrode phonons (0–18 meV). Only low-frequency vibrational modes (<18 meV) couple directly to electrode phonons. The remaining high-frequency modes (>18 meV) appear as sharp peaks in the power spectrum [Fig. 3(a)]. Work done by current-induced forces in this junction is negligible due to low electrical conductance. The energy increase at 1 V is dominated by Joule heating. It involves mainly vibrational modes with an energy larger than 75 meV. Including the anharmonic vibrational coupling leads to large spectrum broadening [Fig. 3(b)], and an excess heating much smaller than the harmonic case [Fig. 3(c)]. Similar to the Au chain, we observe heating of the vibrational modes below 75 meV. This is a direct result of anharmonic vibrational coupling between different modes.

The real space distribution of kinetic energy per bond at 1 V is shown in Fig. 4(a). It is symmetric due to the symmetry of the junction and the negligible contribution of NC current-induced forces. The bond-length histograms for the different types of bonds in the junction are depicted in Fig. 4(b) for harmonic (lower panel) and full AIMD (upper panel) calculations. The current-induced change of bond length and its standard deviation are summarized in Table I. Comparing the two cases, we find that the excess energy of C-H and C-C bonds is effectively transferred away to the Au-C bond in the presence of anharmonic coupling. This is evidenced from the reduced broadening of C-C and C-H bonds and the enhanced broadening of the Au-C bond in the full AIMD results. As a result, the average Au-C bond length increases by ∼0.2 Å. More interestingly, the Au-C bond distribution shows an obvious skewness, thus the average length is larger than the most probable length. This is an important signature of bond anharmonicity, and can only be probed by the full AIMD calculation.

In experiments, an effective temperature T_{eff} has been obtained from contact lifetimes [31] or two-level conductance fluctuations [32] via an Arrhenius-type rate expression. The T_{eff} has been fitted to a V dependence [4], as $T_{\text{eff}} = \gamma\sqrt{V}$ (zero ambient temperature). For both systems above we do not find the energy distribution among the modes is compatible with an overall effective temperature (cf. Fig. S2 of Ref. [28]). On the other hand, we find a maximum kinetic energy of interatomic Au-Au (Au-C) bonds [cf. Figs. 2(a) and 4(a)] of 7 meV (28 meV) corresponding roughly to ∼80 K (320 K) from $k_B T \sim E_K$, which is comparable to experimental values [31,32] of 75 K (450 K).

In summary, we have presented *ab initio* molecular dynamics calculations of an atomic scale conductor in the presence of an electrical current. We illustrated this approach by studying two prototype molecular conductors and analyzing the subtle interplay between Joule heating, current-induced forces, and anharmonic vibrational coupling among different modes. We found that anharmonic coupling among different modes has an important effect on the energy redistribution both in frequency and in real space. Our study opens the possibility of studying current-induced atomic switches, chemical reactions, and bond ruptures [33,34] beyond simple models.

Acknowledgments. We acknowledge funding support from National Natural Science Foundation of China (Grant No. 21873033), the National Key Research and Development Program of China (Grant No. 2017YFA0403501), the program for HUST academic frontier youth team, and Villum Fonden (Grant No. 00013340). We thank the Shanghai supercomputer center for providing computing resources.

[1] T. Seideman, *Current-Driven Phenomena in Nanoelectronics* (Jenny Stanford Publishing, Singapore, 2016).
[2] E. Pop, Nano Res. **3**, 147 (2010).
[3] M. Galperin, M. A. Ratner, and A. Nitzan, J. Phys.: Condens. Matter **19**, 103201 (2007).
[4] T. N. Todorov, Philos. Mag. B **77**, 965 (1998).
[5] D. R. Ward, D. A. Corley, J. M. Tour, and D. Natelson, Nat. Nanotechnol. **6**, 33 (2011).
[6] Z. Ioffe, T. Shamai, A. Ophir, G. Noy, I. Yutsis, K. Kfir, O. Cheshnovsky, and Y. Selzer, Nat. Nanotechnol. **3**, 727 (2008).
[7] Z. Huang, B. Xu, Y. Chen, M. Di Ventra, and N. Tao, Nano Lett. **6**, 1240 (2006).

[8] C. Schirm, M. Matt, F. Pauly, J. C. Cuevas, P. Nielaba, and E. Scheer, Nat. Nanotechnol. **8**, 645 (2013).
[9] R. H. Smit, C. Untiedt, and J. M. Van Ruitenbeek, Nanotechnology **15**, S472 (2004).
[10] N. Agraït, C. Untiedt, G. Rubio-Bollinger, and S. Vieira, Phys. Rev. Lett. **88**, 216803 (2002).
[11] T. N. Todorov, J. Hoekstra, and A. P. Sutton, Phys. Rev. Lett. **86**, 3606 (2001).
[12] D. Dundas, E. J. McEniry, and T. N. Todorov, Nat. Nanotechnol. **4**, 99 (2009).
[13] T. Frederiksen, M. Brandbyge, N. Lorente, and A.-P. Jauho, Phys. Rev. Lett. **93**, 256601 (2004).
[14] J. T. Lü, M. Brandbyge, and P. Hedegård, Nano Lett. **10**, 1657 (2010).
[15] J. T. Lü, R. B. Christensen, J. S. Wang, P. Hedegård, and M. Brandbyge, Phys. Rev. Lett. **114**, 096801 (2015).
[16] W. Lee, K. Kim, W. Jeong, L. A. Zotti, F. Pauly, J. C. Cuevas, and P. Reddy, Nature (London) **498**, 209 (2013).
[17] M. Tsutsui, T. Morikawa, K. Yokota, and M. Taniguchi, Sci. Rep. **8**, 7842 (2018).
[18] M. Tsutsui, Y.-K. Taninouchi, S. Kurokawa, and A. Sakai, Jpn. J. Appl. Phys. **44**, 5188 (2005).
[19] M. Engelund, J. A. Fürst, A. P. Jauho, and M. Brandbyge, Phys. Rev. Lett. **104**, 036807 (2010).
[20] J.-S. Wang, Phys. Rev. Lett. **99**, 160601 (2007).
[21] N. Bode, S. V. Kusminskiy, R. Egger, and F. von Oppen, Phys. Rev. Lett. **107**, 036804 (2011).
[22] J. T. Lü, M. Brandbyge, P. Hedegård, T. N. Todorov, and D. Dundas, Phys. Rev. B **85**, 245444 (2012).
[23] L. Kantorovich, Phys. Rev. B **98**, 014307 (2018).
[24] F. Chen, K. Miwa, and M. Galperin, J. Phys. Chem. A **123**, 693 (2019).
[25] J. T. Lü, B. Z. Hu, P. Hedegård, and M. Brandbyge, Prog. Surf. Sci. **94**, 21 (2019).
[26] T. Frederiksen, M. Paulsson, M. Brandbyge, and A.-P. Jauho, Phys. Rev. B **75**, 205413 (2007).
[27] We use SIESTA [35], TRANSIESTA [36], INELASTICA [26], and the method described in Ref. [37] to get the electronic, vibrational spectrum, electron-vibration, and vibration-electron-phonon coupling. For the MD, we use the I-PI software [38].
[28] See Supplemental Material at http://link.aps.org/supplemental/10.1103/PhysRevB.101.201406 for the validation of the method and numerical details of the calculation.
[29] In order to clearly observe the effect we have excluded the change of the atomic structure and thus the bond length [39].
[30] Z. L. Cheng, R. Skouta, H. Vazquez, J. R. Widawsky, S. Schneebeli, W. Chen, M. S. Hybertsen, R. Breslow, and L. Venkataraman, Nat. Nanotechnol. **6**, 353 (2011).
[31] M. Tsutsui, M. Taniguchi, and T. Kawai, Nano Lett. **8**, 3293 (2008).
[32] M. Tsutsui, S. Kurokawa, and A. Sakai, Appl. Phys. Lett. **90**, 133121 (2007).
[33] A. Erpenbeck, C. Schinabeck, U. Peskin, and M. Thoss, Phys. Rev. B **97**, 235452 (2018).
[34] I. V. Pobelov, K. P. Lauritzen, K. Yoshida, A. Jensen, G. Meszaros, K. W. Jacobsen, M. Strange, T. Wandlowski, and G. C. Solomon, Nat. Commun. **8**, 15931 (2017).
[35] J. M. Soler, E. Artacho, J. D. Gale, A. García, J. Junquera, P. Ordejón, and D. Sánchez-Portal, J. Phys.: Condens. Matt. **14**, 2745 (2002).
[36] M. Brandbyge, J. L. Mozos, P. Ordejón, J. Taylor, and K. Stokbro, Phys. Rev. B **65**, 165401 (2002).
[37] M. Engelund, M. Brandbyge, and A. P. Jauho, Phys. Rev. B **80**, 045427 (2009).
[38] V. Kapil, M. Rossi, O. Marsalek, R. Petraglia, Y. Litman, T. Spura, B. Cheng, A. Cuzzocrea, R. H. Meißner, D. M. Wilkins, B. A. Helfrecht, P. Juda, S. P. Bienvenue, W. Fang, J. Kessler, I. Poltavsky, S. Vandenbrande, J. Wieme, C. Corminboeuf, T. D. Kühne *et al.*, Comput. Phys. Commun. **236**, 214 (2019).
[39] M. Brandbyge, K. Stokbro, J. Taylor, J. L. Mozos, and P. Ordejón, Phys. Rev. B **67**, 193104 (2003).